Available online at www.sciencedirect.com
ScienceDirect
Trans. Nonferrous Met. Soc. China 33(2023) 46−58
Transactions of Nonferrous Metals Society of China
www.tnmsc.cn

Effects of trace Ca addition on microstructure and mechanical properties of as-cast Mg−Sm−Gd-based alloy

Kai GUAN[1,2], Jing-huai ZHANG[1], Qiang YANG[2], Bai-shun LI[3], Rui-zhi WU[1], Jian MENG[2]

1. Key Laboratory of Superlight Material and Surface Technology, Ministry of Education, College of Material Science and Chemical Engineering, Harbin Engineering University, Harbin 150001, China;
2. State Key Laboratory of Rare Earth Resource Utilization, Changchun Institute of Applied Chemistry, Chinese Academy of Sciences, Changchun 130022, China;
3. School of Mechanical and Automotive Engineering, Changchun Institute of Technology, Changchun 130012, China

Received 26 September 2021; accepted 5 January 2022

Abstract: The effects of trace amounts of Ca on the microstructure and mechanical properties of as-cast Mg−Sm−Gd−Zn−Zr alloy were systematically investigated mainly by means of transmission electron microscopy (TEM), high-angle annular dark-field scanning transmission electron microscopy (HAADF-STEM) and tensile test. The results reveal that the dominant intermetallic compound in Mg−Sm−Gd−Zn−Zr alloy is Mg_3RE phase with significant enrichment of Zn. The addition of Ca in Mg−Sm−Gd−Zn−Zr alloy can not only refine grains, but also promote the formation of Mg_5RE phase and solute-enriched stacking faults (SESFs). The coherent interface indicates that Mg_3RE phase can act as the nucleation site of Mg_5RE phase. Finally, the decreased grain size and the formation of Mg_5RE phase and SESFs in the Ca-modified alloy are beneficial to the enhancement of mechanical properties.

Key words: Mg−Sm−Gd alloy; Ca; microstructure characterization; mechanical properties; transmission electron microscopy (TEM)

1 Introduction

Due to low density, magnesium (Mg) alloys with high specific strength have great potential in transportation and aerospace industries [1−5]. Nevertheless, compared with steel, titanium alloys and aluminum alloys, conventional Mg alloys have relatively low mechanical properties, which gravely limits their practical applications. A great number of works demonstrated that rare earth (RE) elements can significantly improve the mechanical properties of Mg alloys by optimizing microstructure [6−12].

Great efforts have been made to develop high-performance Mg−RE-based alloys. As a typical less-expensive RE element, samarium (Sm) has attracted considerable attention in recent years, because it has the largest maximum solid solubility (5.8 wt.%) in Mg among the light RE elements [13−20]. It is widely known that, zinc (Zn) can effectively promote ageing precipitation [2,3], and zirconium (Zr) can remarkably refine grain size [11−13], which is conducive to improving the mechanical properties of Mg alloys. Therefore, Mg−Sm−Zn−Zr quaternary alloy considered to be one of the most promising candidates for high-performance Mg alloy with relatively low contents of RE has been becoming a focus in Mg−Sm alloy system. Among various Mg−Sm−Zn−Zr alloys with different compositions,

Corresponding author: Jing-huai ZHANG, E-mail: jinghuaizhang@gmail.com; Qiang YANG, E-mail: qiangyang@ciac.ac.cn; Bai-shun LI, E-mail: bsli@ciac.ac.cn
DOI: 10.1016/S1003-6326(22)66089-8

Mg−3.5Sm−0.6Zn−0.5Zr alloy shows optimized mechanical properties. The tensile yield strength of the extruded sample is 363 MPa at room temperature, which is further increased to 416 MPa after aging treatment [17,18]. It is important to note that, compared with the frequently reported Mg alloys containing heavy RE elements such as gadolinium (Gd) and yttrium (Y), the aging strengthening effect in Mg−Sm−Zn−Zr alloy is insufficient because of the limitation of solid solubility of Sm in Mg matrix.

ROKHLIN et al [21,22] proposed that the combined addition of RE elements belonging to different sub-groups (Ce sub-group and Y sub-group) can change the precipitation kinetics and accelerate the decomposition of the supersaturated Mg solid solution, and then enhance the aging hardening effect of Mg−RE-based alloys. With the purpose of further enhancing the ageing strengthening effect, a typical Y sub-group RE element, Gd, is generally selected to be added into Mg−Sm-based alloy, since its solid solubility in Mg matrix is 23.3 wt.% at eutectic temperature. Hence, a series of Mg−Sm−Gd based alloys have been developed [23−28]. Apart from a mass of precipitates formed on prismatic planes, a number of precipitates formed on basal planes are revealed in Gd-modified Mg−Sm−Zn−Zr alloys after ageing treatment [24,27]. In this case, the mechanical properties of Mg alloys can be significantly improved at room temperature and elevated temperatures, because both the basal and non-basal dislocation slips can be impeded effectively during plastic deformation [27].

It is widely known that cheap calcium (Ca) with relatively low density (1.55 g/cm^3) can enhance the flame resistance of molten Mg alloys and increase their safe service temperature [29]. Importantly, it is reported that multiple mechanical properties of Mg alloys can be distinctly improved by Ca addition [30−35]. For example, trace Ca can induce the formation of Guinier−Preston (GP) zones and improve the creep property at high temperatures in Mg−Gd−Zn−Zr alloy [31]. In addition, Ca segregation has been observed in precipitates of aged Mg−Gd−Zr alloy, and it was revealed that Ca addition can accelerate the precipitation of β phase [32]. More recently, it has been demonstrated that Gd and Ca solutes in Mg solid solution prefer to form co-clusters, which are expected to provide substantial strengthening effect in Mg−Gd−Ca alloys [33]. It is clear that Ca addition can influence the precipitation behaviors and mechanical properties of Mg alloys, especially Mg−Gd-based alloys. However, the effect of Ca on the microstructure of as-cast Mg−Sm−Gd-based alloy, especially the intermetallic compound, has less been analyzed so far.

It is worth noting that the microstructure and intermetallic compounds play a key role in deciding the mechanical properties and heat resisting property of Mg alloys [36,37]. Therefore, clarifying the detailed information of dominant intermetallic compounds is beneficial to the development of novel high-performance Mg alloys. In the present work, the effects of trace Ca addition on the microstructure and mechanical properties of as-cast Mg−Sm−Gd−Zn−Zr alloy are systematically investigated.

2 Experimental

The alloys with nominal compositions of Mg−3.5Sm−2.0Gd−0.5Zn−0.5Zr−xCa (x=0 and 0.2, wt.%) were prepared with Mg−20wt.%Sm, Mg−25wt.%Gd, Mg−30wt.%Zr and Mg−30wt.%Ca master alloys, and high purity Mg and Zn in an electric resistance furnace. The raw materials were melted at about 760 °C in a steel crucible under the protection of gas mixture (1 vol.% SF_6 and 99 vol.% CO_2). After being fully stirred, the melt was kept still at about 740 °C for 0.5 h. Finally, the melt was poured into a preheated permanent mold. The tensile and compressive tests were performed on Instron 5869 testing machine with an initial strain rate of 1.0×10^{-3} s^{-1} at room temperature. The gage dimensions of tensile and compressive specimens were d6 mm × 36 mm and d10 mm × 18 mm, respectively.

Inductively coupled plasma atomic emission spectroscopy (ICP-AES) was performed to test actual chemical compositions of the studied alloys, and the corresponding result is listed in Table 1. Microstructural features of these alloys were characterized by optical microscopy (OM, Olympus−GX71), X-ray diffractometer (XRD, Bruker D8 FOCUS) with Cu K_α radiation (λ= 0.15406 nm), scanning electron microscopy (SEM, Hitachi S−4800) equipped with energy-dispersive X-ray spectroscopy (EDS), transmission electron

microscopy (TEM, FEI Tecnai G^2 F20) equipped with EDS operating at 200 kV, and atomic-resolution aberration-corrected scanning transmission electron microscope (STEM, FEI Taitan^3 TM G^2 60−300) operating at 300 kV. The accelerating voltage and working distance for collecting backscattered SEM micrographs were set as 15 kV and 8 mm, respectively. For atomic-resolution high-angle annular dark field scanning transmission electron microscopy (HAADF-STEM) observations, the beam convergence semi-angle was set as 25 mrad and high-angle annular dark field detector ranged from 60 to 290 mrad to obtain atomic number (Z)-contrast images. After mechanical grinding with different grades of SiC emery papers, thin foils with a diameter of 3 mm for TEM/STEM characterizations were ion-milled using precision ion polishing system (PIPS, Gatan 691) equipped with liquid nitrogen cooling system. The cubic specimens used for OM and SEM observations were etched in a mixed solution of ethanol, acetic acid and picric acid after mechanically polishing. Nano Measure 1.2 software was used to roughly measure the grain size of the present samples based on five OM images.

Table 1 Actual chemical compositions of present alloys (wt.%)

Alloy	Sm	Gd	Zn	Zr	Ca	Mg
SG	3.39	2.07	0.47	0.45	−	Bal.
SGX	3.46	2.02	0.44	0.41	0.17	Bal.

3 Results and discussion

3.1 Microstructure evolution

Figures 1(a, b) show the low-magnification OM images of as-cast Mg−3.5Sm−2Gd−0.5Zn−0.5Zr (SG) and Mg−3.5Sm−2Gd−0.2Ca−0.5Zn−0.5Zr (SGX) alloys. The equiaxed Mg grains and distinct grain boundaries can be seen in both alloys. In order to investigate the influence of Ca on the grain refinement in the present alloys, Nano Measure 1.2 software was used to estimate the average grain size. The results are shown in Figs. 1(c, d). The average grain sizes of SG and SGX alloys are (44.2±6.2) and (39.5±5.7) μm, respectively, indicating that Ca can effectively refine the grains of Mg−Sm−Gd−Zn−Zr alloys. In general, grain refinement effect of as-cast alloys can be ascribed to the constitutional supercooling induced by accumulation of solute atoms in front of the liquid/solid interface during solidification. According to previous reports [38,39], the grain refining effect can be briefly represented by the growth-restriction parameter, Q, which is described as

$$Q=mC_0(k-1) \quad (1)$$

where m is the liquidus slope, C_0 is the solute concentration in the alloy melt and k is the solute partition coefficient. It is clear that solute concentration plays an important role in grain growth-restriction. In the present alloy system, the addition of Ca leads to an increment of solute concentration, which can further induce the enhancement of constitutional supercooling in the liquid region ahead of an advancing Mg solid front, and consequently promote nucleation in liquid region and refine grains. Figures 1(e, f) show the backscattered SEM images of as-cast SG and SGX alloys, respectively. Numerous blocky and rod-like intermetallic compounds with bright contrast are frequently observed at grain boundaries in both alloys. Meanwhile, some particulate phases are sporadically observed in grain interiors and at boundaries. By further inspection of these images, significant contrast is also observed within grains close to grain boundaries, although there is no intermetallic distribution at some grain boundaries, implying that the concentration of solute atoms near grain boundary is larger than that inside grains. Similar phenomenon known as micro-segregation is attributed to non-equilibrium solidification and dendrite tip undercooling [13,40,41]. It should be noted that, in addition to the dominant bright phase, a rod-like phase with grey contrast (indicated by a yellow arrow in Fig. 1(f)) is observed in SGX alloy, suggesting that a new phase is formed in the Ca-modified alloy.

As shown in Fig. 2, XRD was carried out to investigate the intermetallic compounds in the present alloys. In both alloys, besides the main diffraction peaks representing the Mg lattice, some extra diffraction peaks originating from inter-metallic compounds are obviously observed in the XRD patterns. All the additional diffraction peaks in the SG alloy and most of those in SGX alloy can be indexed by face centered cubic (fcc) Mg_3RE phase. However, a faint diffraction peak around

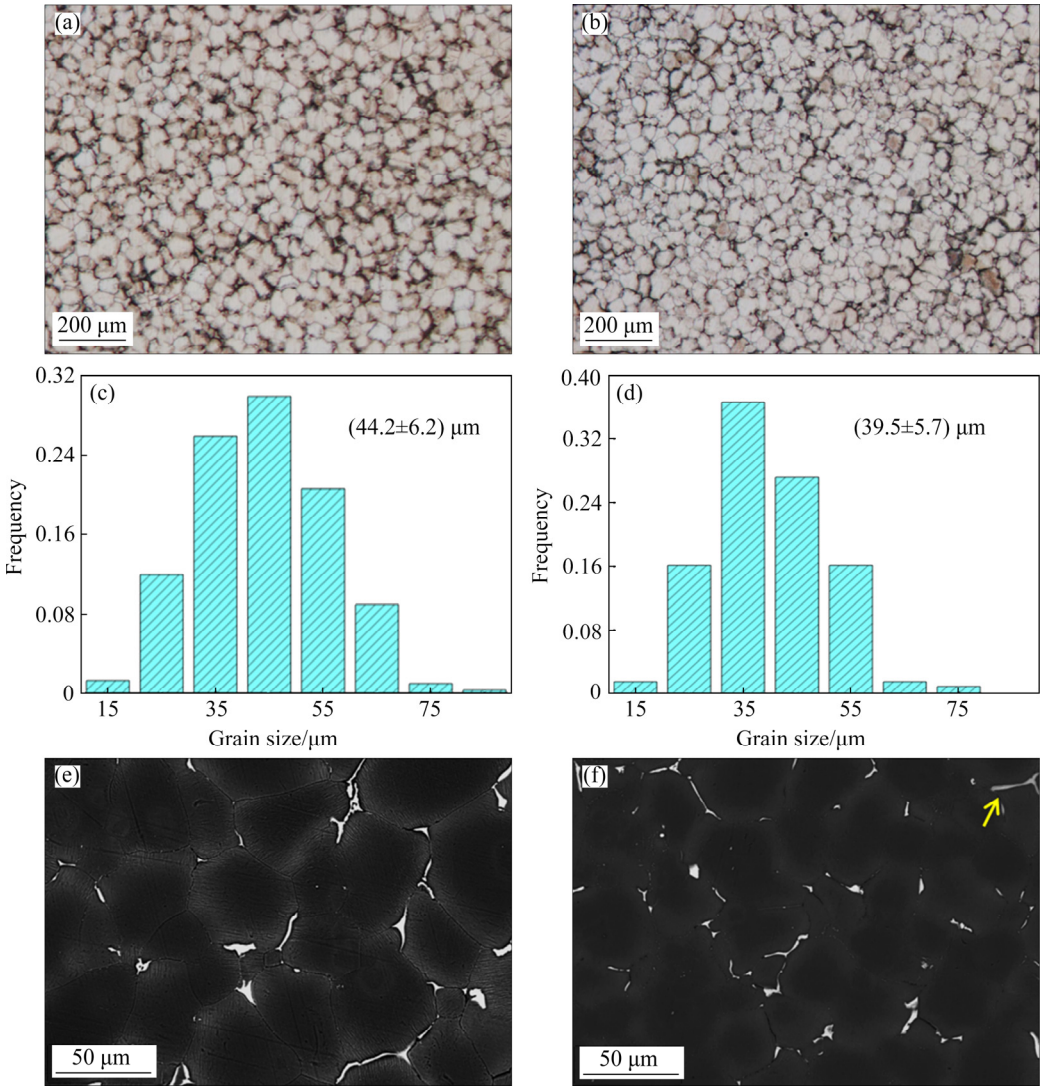

Fig. 1 OM images (a, b), histograms of grain size distribution (c, d) and SEM images (e, f) of SG (a, c, e) and SGX (b, d, f) alloys

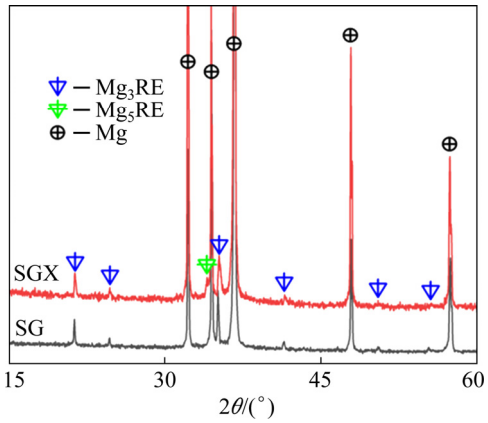

Fig. 2 XRD patterns of as-cast SG and SGX alloys

2θ=35° in SGX alloy cannot be identified by Mg_3RE, which can be indexed by fcc Mg_5RE phase. This implies that the grey phase in SGX alloy (Fig. 1(f)) may be Mg_5RE phase.

3.2 TEM characterizations of intermetallic compounds

TEM was performed to precisely investigate the crystal structures of these intermetallic compounds in both alloys. The typical bright field (BF) TEM image of a blocky phase in SG alloy is shown in Fig. 3(a). Based on the selected area electron diffraction (SAED) pattern (Fig. 3(b)) corresponding to the region marked with a white dotted circle in Fig. 3(a), blocky phase is identified as fcc Mg_3RE phase with lattice parameter of a=0.7193 nm, which is further supported by the fast Fourier transform (FFT) pattern (Fig. 3(d)) generated from the high-resolution (HR) TEM image shown in Fig. 3(c). It is worth mentioning that the experimental lattice parameter of Mg_3RE phase in SG alloy is smaller than that in binary

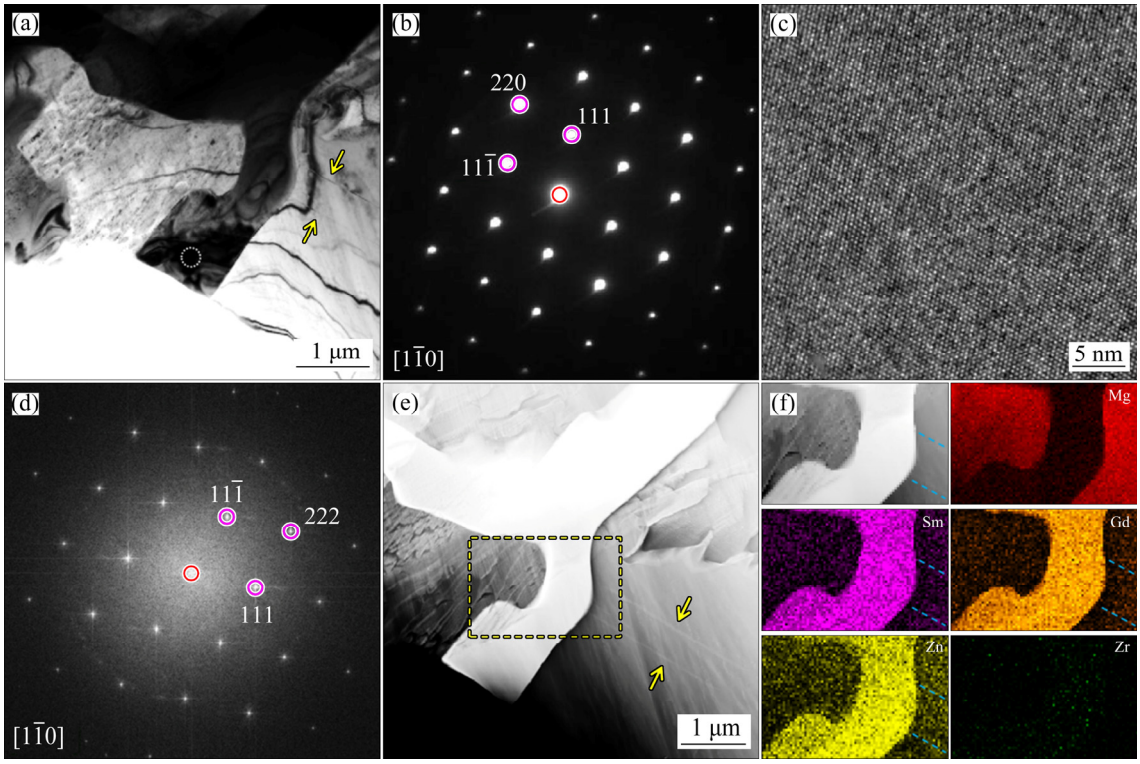

Fig. 3 BF-TEM image (a), SAED pattern (b) and HR-TEM image (c) of representative blocky intermetallic compound in SG alloy; (d) FFT pattern generated from (c); (e) Corresponding HAADF-STEM image; (f) EDS mappings of yellow dashed rectangle region

Mg−Gd alloy (a=0.7324 nm) [42] and Mg−Sm alloy (a=0.7346 nm) [43]. Figure 3(f) presents the EDS mappings of the yellow dotted rectangle region in the relevant HAADF-STEM image shown in Fig. 3(e). It can be seen that, in addition to Sm and Gd, Zn is significantly segregated in the blocky phase. The decreased lattice parameter of Mg_3RE phase can be attributed to Zn segregation since the atomic radius of Zn (0.137 nm) is much smaller than that of Mg (0.160 nm), Sm (0.180 nm) and Gd (0.180 nm). By the way, fibrous structure with large aspect ratio is rarely observed in the Mg matrix, as indicated by yellow arrows in Figs. 3(a, e). More interestingly, further examination of the EDS mappings shown Fig. 3(f) reveals that Sm, Gd and Zn are slightly segregated in the fibrous structure, as indicated by cyan dotted lines. It can be deduced that the fibrous structure may be stacking fault with the segregation of Sm, Gd and Zn alloying elements.

The representative BF-TEM image of the sandwich-type intermetallic compound in SGX alloy is shown in Fig. 4(a), in which the inset of SAED pattern is obtained from Region A indicated by a white dotted circle. The SAED patterns corresponding to Regions B (indicated by a purple dotted circle) and C (indicated by a yellow dotted circle) in Fig. 4(a) are present in Figs. 4(c, d), respectively. The HR-TEM image corresponding to Region A in Fig. 4(a) is presented in Fig. 5(a), in which an interface (highlighted by cyan lines) is distinctly observed. The FFT patterns generated from the yellow and purple dotted rectangles in Fig. 5(a) are presented in Figs. 5(b, c), respectively. By analyzing these SAED and FFT patterns, the sandwiched and adjacent intermetallic compounds are demonstrated as Mg_3RE phase (fcc, a= 0.7297 nm) and Mg_5RE phase (fcc, a=2.2556 nm), respectively. Their orientation relationship is $(111)_{Mg_5RE}//(111)_{Mg_3RE}$ and $[1\,\bar{1}0]_{Mg_5RE}//[1\,\bar{1}0]_{Mg_3RE}$.

The typical HAADF-STEM image is shown in Fig. 6(a), and the relevant EDS mappings of the partial sandwich-type intermetallic compound marked with a yellow dotted rectangle are shown in Figs. 6(b−g). It is clear that Sm, Gd and Zn are remarkably segregated in the sandwiched layer (Mg_3RE phase), whereas their segregations in the adjacent layers (Mg_5RE phase) are much weak. It is

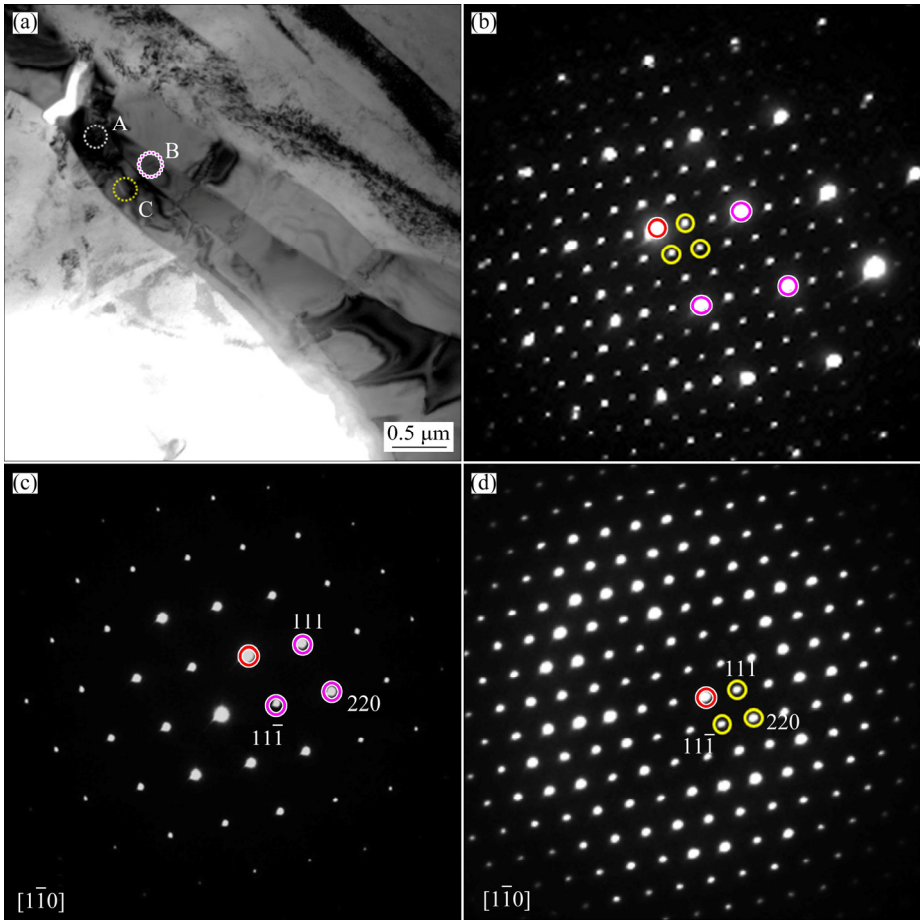

Fig. 4 BF-TEM image (a) of sandwich-type intermetallic compound in SGX alloy, and SAED patterns corresponding to Regions A (b), B (c) and C (d) marked in (a)

important to notice that Ca segregation in the adjacent layers (Mg_5RE phase) is much richer than that in the sandwiched layer (Mg_3RE phase), suggesting that Ca addition induces the formation of Mg_5RE phase in the present Mg−Sm−Gd−Zn−Zr alloy. Similar to the Mg_3RE phase in SG alloy, the lattice parameter (a=0.7297 nm) of Mg_3RE phase in SGX alloy is smaller than the standard value in binary Mg−Sm/Gd alloys due to the significant segregation of Zn. But it is slightly larger than that in SG alloy, which can be attributed to the slight segregation of Ca that has relatively large atomic radius (0.197 nm) in the Mg_3RE phase for SGX alloy. It is remarkably known, however, that the experimental lattice parameter (a=2.2556 nm) of Mg_5RE phase in SGX alloy is larger than that in binary Mg−Gd alloy (a=2.235 nm) [42] and Mg−Sm alloy (a=2.246 nm) [43]. This is because Ca with large atomic radius (0.197 nm) is significantly enriched in the Mg_5RE phase while Zn with small atomic radius (0.137 nm) is relatively scarce, as shown in Figs. 6(e, f). The coherent interface shown in Fig. 5(a) indicates that Mg_3RE phase can act as nucleation site of Mg_5RE phase.

For the sake of further verification, another region where Mg_3RE phase and Mg_5RE phase coexist was characterized by TEM along a different beam incidence direction. The BF-TEM image shown in Fig. 7(a) displays a blocky intermetallic compound with different contrast. The SAED pattern taken from the interface around Region A (indicated by a white dotted circle) is shown in Fig. 7(b). Figures 7(c, d) present the SAED patterns obtained from Regions B (indicated by a purple dotted circle) and C (indicated by a yellow dotted circle) in Fig. 7(a), respectively. The inner and outer layers are definitely indexed by Mg_3RE phase and Mg_5RE phase viewed from [11$\bar{2}$] zone axis, respectively. This suggests that Ca-enriched Mg_5RE phase generally prefers to nucleate at the tip of Mg_3RE phase during solidification, being well consistent with the result shown in Figs. 4 and 5.

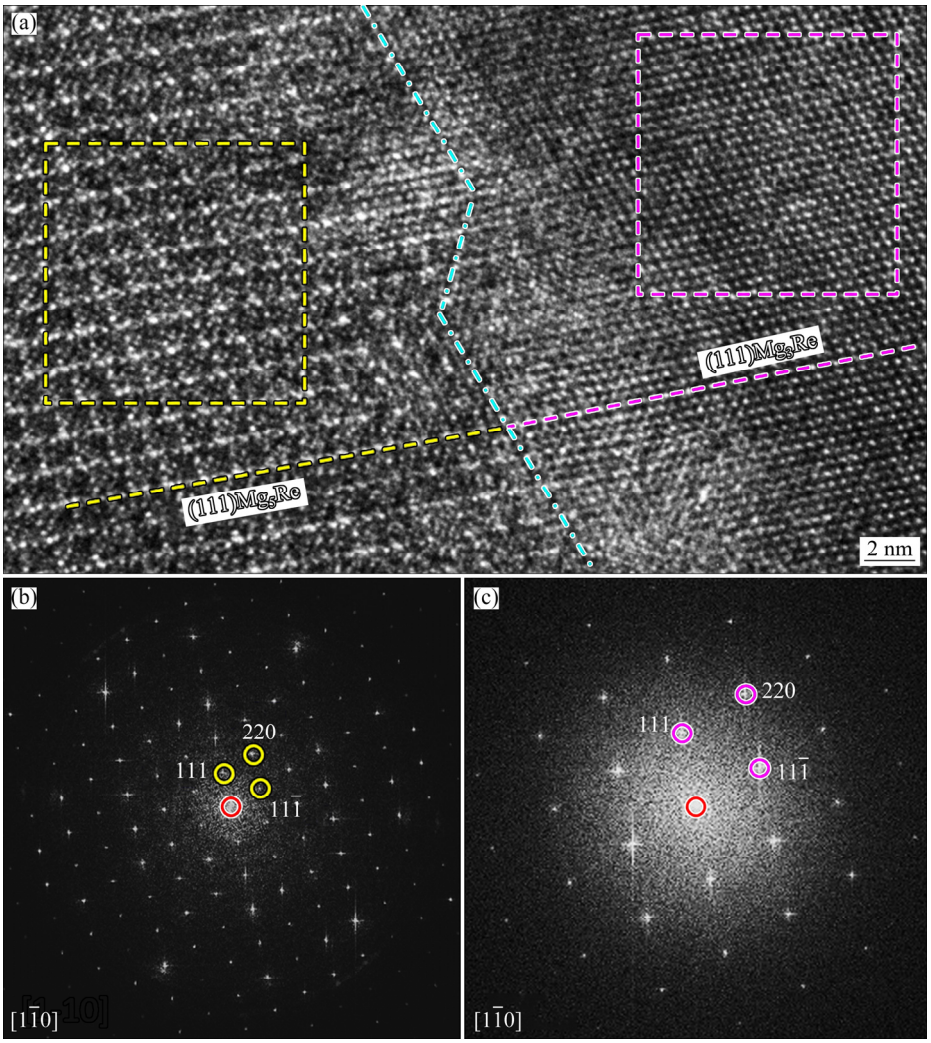

Fig. 5 HR-TEM image of SGX alloy (a), and FFT patterns generated from yellow (b) and pink (c) dashed rectangle regions highlighted in (a)

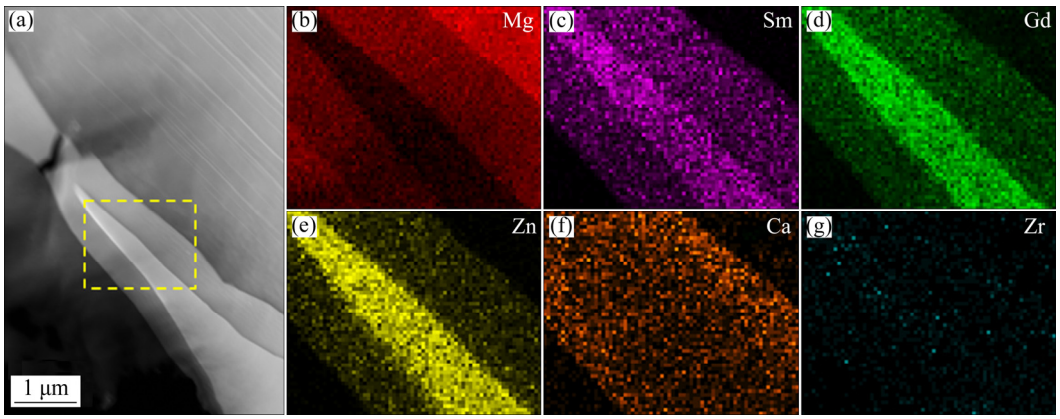

Fig. 6 HAADF-STEM image (a) of sandwich-type intermetallic compound in SGX alloy, and EDS mappings (b−g) of yellow dashed rectangle region in (a)

Another critical fact to notice is that lamellar structures distributed in the Mg matrix are continually observed in SGX alloy, whereas they are extremely rare in SG alloy. Figure 8(a) gives the representative BF-TEM image of the Mg matrix in SGX alloy, from which plenty of lamellar structures distributed parallel to each other are observed. The diffusion streaks are obviously displayed along *c*

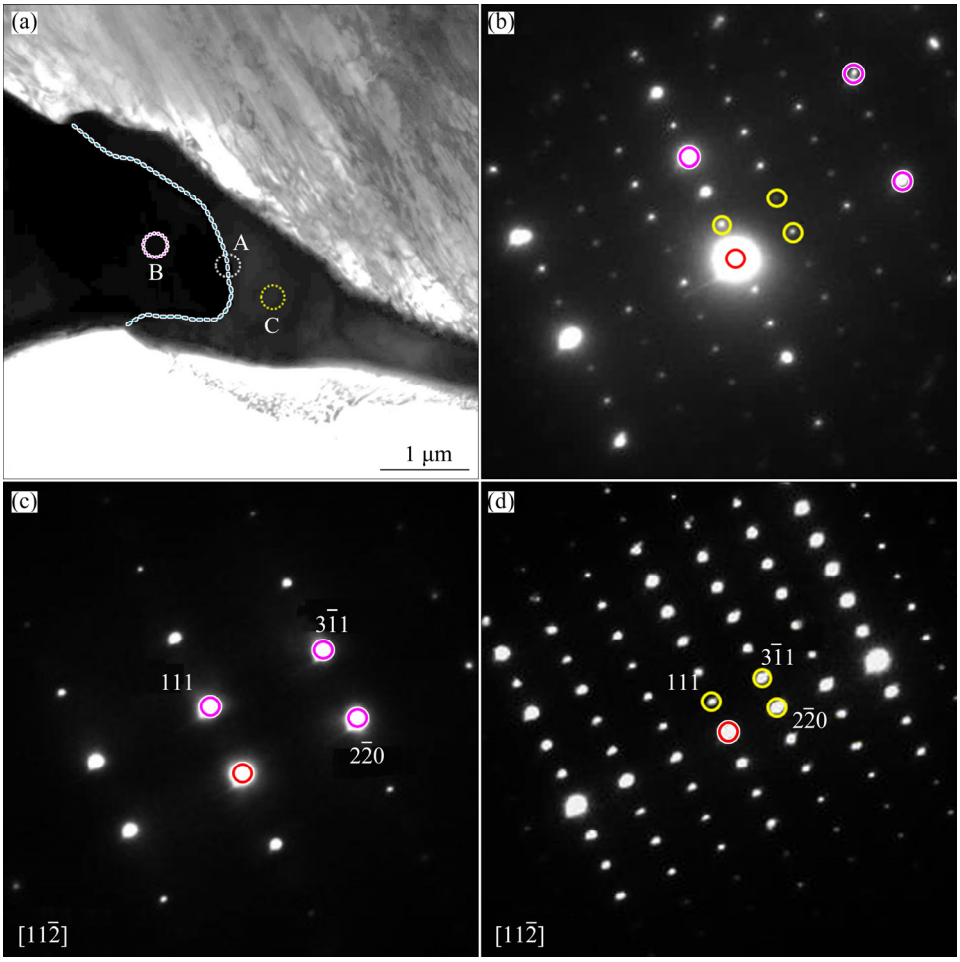

Fig. 7 BF-TEM image (a) of typical blocky phase in SGX alloy, and SAED patterns corresponding to Regions A (b), B (c) and C (d) marked in (a)

direction in the corresponding SAED pattern presented in Fig. 8(b), which indicates that these lamellar structures are formed on basal plane in the Mg matrix. As shown in Fig. 8(c), these lamellar structures exhibit much stronger *Z*-contrast than Mg matrix in the low-magnification HAADF-STEM image, implying the segregation of alloying elements.

In order to reveal the detailed configuration of lamellar structure, atomic-resolution characterization was performed. The typical atomic-resolution HAADF-STEM image of lamellar structures is presented in Fig. 8(d). It is evident that the lamellar structures can be identified as intrinsic II (I_2)-type solute enriched stacking faults (SESFs) constructed by AB′C′A-stacking unit with local fcc configuration. As indicated by purple rectangular-bar in Fig. 8(d), the shear direction of AB′C′A stacking sequence in each two adjacent SESFs is different, caused by the odd number (5 and 3) of the sandwiched Mg layers. The corresponding *Z*-contrast intensity profile (orange curve attached in Fig. 8(d)) reveals that four-layered SESFs contain two inner layers with significant segregation and two outer layers with intermediate segregation, which agrees well with the structural feature of LPSO phase in Mg−Zn−RE alloys. Furthermore, a certain number of dots exhibiting the brightest contrast can be picked out in the middle two layers of SFSFs, which are marked by yellow dotted circles in Fig. 8(d). These particular configurations appear to be short range order (SRO) clusters, which are believed to play a critical role in improving the thermostability of LPSO phase and SESFs in Mg−Zn−RE alloys [6]. The representative HAADF-STEM image along with the EDS mappings of SESFs are shown in Fig. 9. It can be seen that, in addition to Sm, Gd and Zn elements, Ca is distinctly segregated in the SESFs, suggesting that Ca addition can promote SESFs formation in

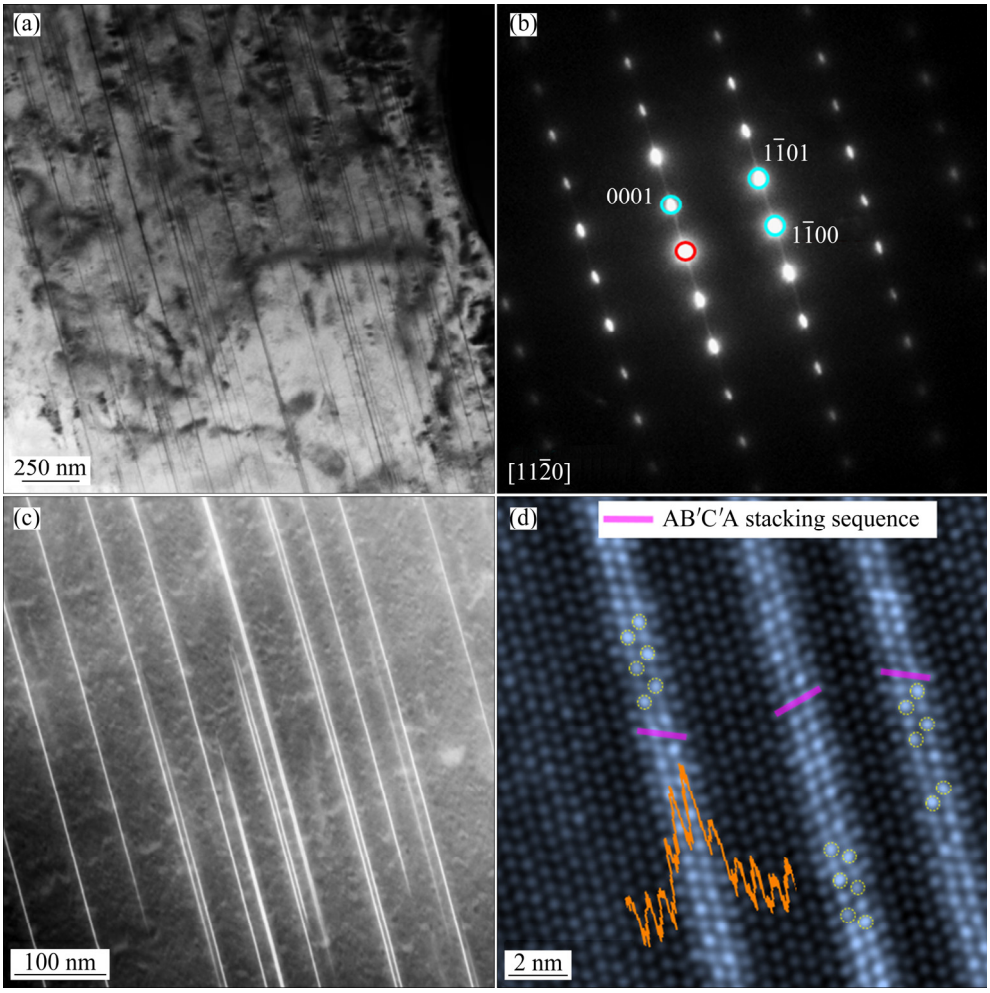

Fig. 8 BF-TEM image (a), SAED pattern (b), HAADF-STEM image (c) and typical atomic-resolution HAADF-STEM image (d) of lamellar structures in SGX alloy

the present Mg−Sm−Gd−Zn−Zr alloy. This may be attributed to two factors. On one hand, Ca segregation reduces the formation energy of SESFs and on the other hand, Ca segregation releases the elastic strain caused by SESFs formation. CHEN et al [32] proposed that Ca segregation can reduce the nucleation barrier of β phase and decrease the formation energy of β' phase in Mg−15Gd−0.5Zr−0.6Ca alloy. It should be pointed out that the specific mechanism of Ca promoting SESFs formation requires further study.

3.3 Mechanical properties

The typical tensile and compressive curves at room temperature are shown in Figs. 10(a, b), respectively. For tensile tests (Fig. 10(a)), the yield strength (YS), ultimate strength (US) and elongation (EL) of SG alloy are 105.6 MPa, 135.1 MPa and 5.8%, respectively. The YS, US and EL are improved to 115.1 MPa, 146.7 MPa and 6.6% for SGX alloy, respectively. Similarly, from compressive tests (Fig. 10(b)), the YS, US and EL of SGX are increased from 97.7 MPa, 163.3 MPa and 6.7% of SG alloy to 110.4 MPa, 189.9 MPa and 7.3%, respectively. It is obvious that trace Ca can effectively enhance both the strength and ductility of Mg−Sm−Gd−Zn−Zr alloy.

In as-cast Mg alloys, the enhancement of mechanical properties can be generally attributed to grain refinement strengthening, second phase strengthening, solid solution strengthening and precipitation strengthening. Firstly, the grain refinement strengthening effect can be estimated according to the Hall−Petch relation [44]:

$$\Delta\sigma_{gs}=k'd^{-1/2} \quad (2)$$

where k' is a constant, and d represents the average grain size. As shown in Figs. 1(c, d), the average

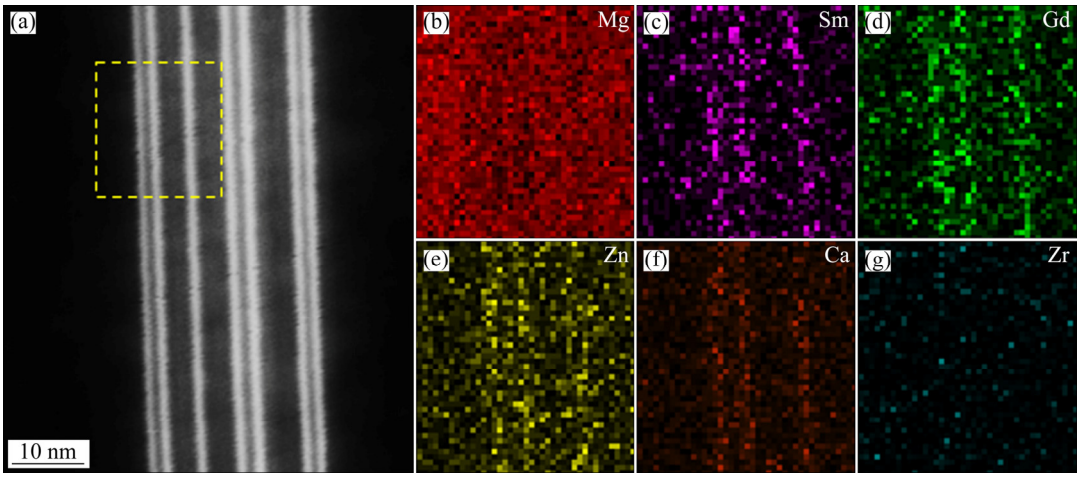

Fig. 9 HAADF-STEM image (a) of lamellar structures in SGX alloy, and EDS mappings corresponding to yellow dashed rectangle region (b−g)

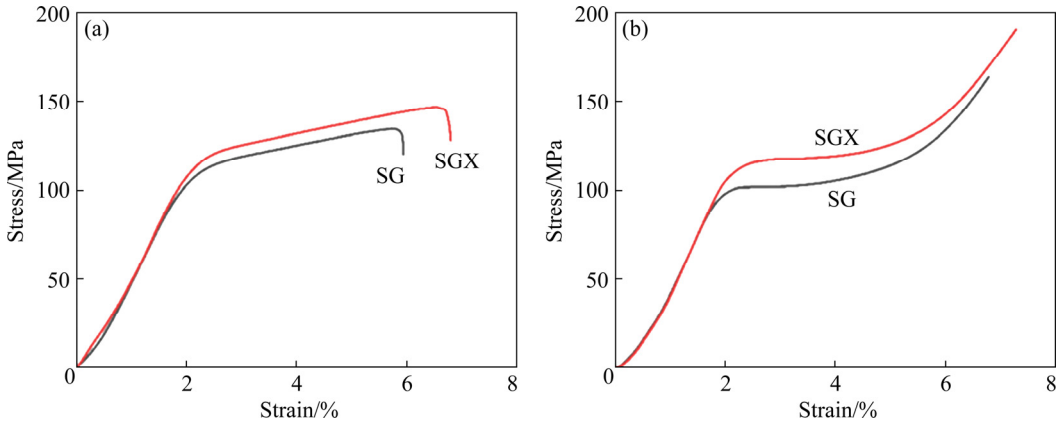

Fig. 10 Tensile (a) and compressive (b) curves of present alloys

grain size of SGX alloy is smaller than that of SG alloy, indicating that the grain refinement strengthening effect in SGX alloy is greater than that in SG alloy. In addition, the relatively small grain size of SGX alloy provides a good explanation for the increased ductility.

Secondly, the RE-containing second phase distributed at grain boundaries can remarkably impede grain boundary movement during plastic deformation, thus enhancing the strength of alloy. It was demonstrated that the strengthening effect of second phases is primarily dependent upon their crystal structures and volume fractions [36,37]. In the present alloys, both the Mg_3RE and Mg_5RE phases have fcc crystal structure, implying the volume fraction of intermetallic compounds plays a critical role in second phase strengthening. It should be noted the percentage of RE atoms in Mg_5RE phase is smaller than that in Mg_3RE phase. As displayed in Table 1, the contents of Sm and Gd in SG alloy and SGX alloy are almost equal. As we have demonstrated in previous sections, the dominant second phase in SG alloy is Mg_3RE phase, while in SGX alloy Mg_5RE phase is distinctly observed in addition to Mg_3RE phase. It is reasonable to infer that the volume fraction of intermetallic compounds in SGX alloy is larger than that in SG alloy. Accordingly, SGX alloy exhibits better second phase strengthening effect than SG alloy.

Thirdly, solute atoms segregated in the matrix can effectively restrain dislocation slip during plastic deformation and thus improve the strength of alloy. The solid solution strengthening effect can be calculated by [44]

$$\Delta\sigma_{ss} = C_i X_i^{2/3} \tag{3}$$

where C_i is a constant for element i, X_i is the molar fraction of solute i. The solid solution strengthening effect originating from Sm, Gd and Zn solute atoms

in SG alloy is considered to be identical to that in SGX alloy because of the equivalent contents of elements. Significantly, although the solid solubility of Ca in Mg is very small, a few Ca atoms must inevitably be segregated in the matrix of SGX alloy, thus providing some additional strengthening.

The last but not the least, as shown in Fig. 8, some lamellar precipitates named as SESFs are formed on basal planes of the matrix in SGX alloy. It has been reported that SESFs are effective in inhibiting gliding dislocations during plastic deformation, thereby enhancing the mechanical properties of Mg alloys [6]. The precipitation strengthening effect of basal precipitates with large aspect ratio can be estimated by the modified Orowan equation [45]:

$$\Delta\sigma_{\mathrm{p}}=\frac{MGb}{2\pi\sqrt{1-\nu}\left(0.953/\sqrt{f}-1\right)d_{\mathrm{t}}}\times\ln\frac{d_{\mathrm{t}}}{b} \tag{4}$$

where M is Taylor factor, G is the shear modulus of Mg, b is the magnitude of Burgers vector, ν is Poisson ratio, and f and d_{t} represent the volume fraction and the uniform diameter of precipitates, respectively. Apparently, the improvement of YS is positively associated with the volume fraction (f) of precipitates. A series of microstructural characterizations by means of TEM reveal the fact that SESFs are frequently observed in SGX alloy and rarely in SG alloy. As a result, the precipitation strengthening effect of SGX alloy is certainly greater than that of SG alloy.

It can be concluded from the above discussion that Ca addition can refine the grains of SGX alloy and promote the formation of Mg_5RE phase and SESFs, which are conducive to the enhancement of mechanical properties. Therefore, Ca can be considered as one of the most promising candidates for modifying the microstructure and optimizing the mechanical properties of Mg−Sm−Gd-based alloy.

4 Conclusions

(1) The dominant intermetallic compound in Mg−Sm−Gd−Zn−Zr alloy is Zn-enriched Mg_3RE phase, whose lattice parameter is smaller than the standard values in Mg−RE binary alloys due to the significant segregation of Zn with relatively small atomic radius (0.137 nm).

(2) In addition to Mg_3RE phase, Ca-enriched Mg_5RE phase and SESFs are frequently observed in Ca-modified alloy, suggesting that Ca promotes the formation of Mg_5RE phase and SESFs. The coherent interface indicates that Mg_3RE phase generally acts as the nucleation site of Mg_5RE phase, and their orientation relationship is $(111)_{Mg_5RE}//(111)_{Mg_3RE}$ and $[1\bar{1}0]_{Mg_5RE}//[1\bar{1}0]_{Mg_3RE}$. Because of the remarkable enrichment of Ca with relatively large atomic radius (0.197 nm), the experimental lattice parameter of Mg_5RE phase in the present alloy is distinctly larger than that reported in Mg−Sm and Mg−Gd binary alloys.

(3) The addition of Ca can effectively refine the grains in Mg−Sm−Gd−Zn−Zr alloy. Both the strength and ductility of tensile and compressive tests at room temperature are improved by Ca addition in the present alloys.

Acknowledgments

This work was supported by the National Natural Science Foundation of China (No. 52071093, 51871069), the Fundamental Research Funds for the Central Universities, China (No. 3072021CF1008), and the Open Funds of the State Key Laboratory of Rare Earth Resource Utilization, China (No. RERU2020012).

References

[1] YANG Qiang, YAN Zi-xiang, LV Shu-hui, GUAN Kai, QIU Xin. Abnormal creep stress exponents in a high-pressure die casting Mg−Al−RE alloy [J]. Materials Science and Engineering A, 2022, 831: 142203.

[2] NIE J F, GAO X, ZHU S M. Enhanced age hardening response and creep resistance of Mg−Gd alloys containing Zn [J]. Scripta Materialia, 2005, 53: 1049−1053.

[3] HONMA T, OHKUBO T, KAMADO S, HONO K. Effect of Zn additions on the age-hardening of Mg−2.0Gd−1.2Y−0.2Zr alloys [J]. Acta Materialia, 2007, 55: 4137−4150.

[4] FU Peng-huai, WANG Nan-qing, LIAO Hai-guang, XU Wen-yu, PENG Li-ming, CHEN Juan, HU Guo-qi, DING Wen-jiang. Microstructure and mechanical properties of high strength Mg−15Gd−1Zn−0.4Zr alloy additive-manufactured by selective laser melting process [J]. Transactions of Nonferrous Metals Society of China, 2021, 31: 1969−1978.

[5] LIU Ke, LIU Jin-xue, LI Shu-bo, WANG Zhao-hui, DU Wen-bo, WANG Qing-feng. Effects of secondary phases on texture and mechanical properties of as-extruded Mg−Zn−Er alloys [J]. Transactions of Nonferrous Metals Society of China, 2018, 28: 890−895.

[6] GUAN Kai, EGAMI M, EGUSA D, KIMIZUKA H, YAMASAKI M, KAWAMURA Y, ABE E. Short-range order clusters in the long-period stacking/order phases with an intrinsic-I type stacking fault in Mg−Co−Y alloys [J]. Scripta Materialia, 2022, 207: 114282.

[7] XIE Jin-shu, ZHANG Jing-huai, YOU Zi-hao, LIU Shu-juan, GUAN Kai, WU Rui-zhi, WANG Jun, FENG Jing. Towards developing Mg alloys with simultaneously improved strength and corrosion resistance via RE alloying [J]. Journal of Magnesium and Alloys, 2021, 9: 41−56.

[8] ZHANG Jing-huai, LIU Shu-juan, WU Rui-zhi, HOU Le-gan, ZHANG Mi-lin. Recent developments in high-strength Mg−RE-based alloys: Focusing on Mg−Gd and Mg−Y systems [J]. Journal of Magnesium and Alloys, 2018, 6: 277−291.

[9] LV Shu-hui, LÜ Xiao-ling, MENG Fan-zhi, YANG Qiang, QIU Xin, QIN Peng-fei, DUAN Qian, MENG Jian. Microstructures and mechanical properties in a Gd-modified high-pressure die casting Mg−4Al−3La−0.3Mn alloy [J]. Materials Science and Engineering A, 2020, 773: 138725.

[10] YANG Qiang, LV Shu-hui, YAN Zi-xiang, HUA Xi-ru, QIU Xin, MENG Jian. Nano-steps in long-period stacking ordered structures for ductility asymmetry of a strong-textured Mg−Gd−Zn alloy [J]. Materials & Design, 2021, 201: 109482.

[11] YAN Zi-xiang, YANG Qiang, MENG Fan-zhi, MA Rui, BAO Ri-rong, LIU, Xiao-juan, MENG Jian, QIU Xin. Interfacial precipitation in $\{10\bar{1}2\}$ twin boundaries of a Mg−Gd−Zn−Zr alloy [J]. Journal of Materials Science and Technology, 2021, 93: 103−109.

[12] STJOHN D H, QIAN M, EASTON M A, CAO P, HILDEBRAND Z. Grain refinement of magnesium alloys [J]. Metallurgical and Materials Transactions A, 2005, 36: 1669−1679.

[13] GUAN Kai, MA Rui, ZHANG Jing-huai, WU Rui-zhi, YANG Qiang, MENG Jian. Modifying microstructures and tensile properties of Mg−Sm based alloy via extrusion ratio [J]. Journal of Magnesium and Alloys, 2021, 9: 1098−1109.

[14] GUAN Kai, LI Bai-shun, YANG Qiang, QIU Xin, TIAN Zheng, ZHANG Dong-dong, ZHANG De-ping, NIU Xiao-dong, SUN Wei, LIU Xiao-juan, MENG Jian. Effects of 1.5 wt.% samarium (Sm) addition on microstructures and tensile properties of a Mg−6.0Zn−0.5Zr alloy [J]. Journal of Alloys and Compounds, 2018, 735: 1737−1749.

[15] XIA Xiang-yu, SUN Wei-hua, LUO A A, STONE D S. Precipitation evolution and hardening in Mg−Sm−Zn−Zr alloys [J]. Acta Materialia, 2016, 111: 335−347.

[16] YANG Qiang, GUAN Kai, QIU Xin, ZHANG De-ping, LV Shu-hui, BU Fan-qiang, ZHANG Ya-qin, LIU Xiao-juan, MENG Jian. Structures of Al_2Sm phase in a high-pressure die-cast Mg−4Al−4Sm−0.3Mn alloy [J]. Materials Science and Engineering A, 2016, 675: 396−402.

[17] GUAN Kai, MENG Fan-zhi, QIN Peng-fei, YANG Qiang, ZHANG Dong-dong, LI Bai-shun, SUN Wei, LV Shu-hui, HUANG Yuan-ding, HORT N, MENG Jian. Effects of samarium content on microstructure and mechanical properties of Mg−0.5Zn−0.5Zr alloy [J]. Journal of Materials Science and Technology, 2019, 35: 1368−1377.

[18] GUAN Kai, YANG Qiang, BU Fan-qiang, QIU Xin, SUN Wei, ZHANG De-ping, ZHENG Tian, NIU Xiao-dong, LIU Xiao-juan, MENG Jian. Microstructures and mechanical properties of a high-strength Mg−3.5Sm−0.6Zn−0.5Zr alloy [J]. Materials Science and Engineering A, 2017, 703: 97−107.

[19] YANG Qiang, BU Fan-qiang, QIU Xin, LI Yang-de, LI Wei-rong, SUN Wei, LIU Xiao-juan, MENG Jian. Strengthening effect of nano-scale precipitates in a die-cast Mg−4Al−5.6Sm−0.3Mn alloy [J]. Journal of Alloys and Compounds, 2016, 665: 240−250.

[20] GUAN Kai, LI Bai-shun, YANG Qiang, ZHANG Dong-dong, ZHANG Xu-hu, ZHANG Jing-qi, ZHAO Lei, LIU Xiao-juan, MENG Jian. Microstructural characterization of intermetallic phases in a solution-treated Mg−5.0Sm−0.6Zn−0.5Zr (wt.%) alloy [J]. Materials Characterization, 2018, 145: 329−336.

[21] ROKHLIN L L, DOBATKINA T V, NIKITINA N I. Constitution and properties of the ternary magnesium alloys containing two rare-earth metals of different subgroups [J]. Materials Science Forum, 2003, 419/420/421/422: 291−296.

[22] LUK'YANOVA E A, ROKHLIN L L, DOBATKINA T V, KOROL'KOVA I G, TARYTINA I E. Effect of samarium on the properties of Mg−Y−Gd−Zr alloys [J]. Russian Metallurgy, 2018, 1: 51−55.

[23] ZHANG Zhen-yan, PENG Li-ming, ZENG Xiao-qin, FU Peng-huai, DING Wen-jiang. Characterization of phases in a Mg−6Gd−4Sm−0.4Zr (wt.%) alloy during solution treatment [J]. Materials Characterization, 2009, 60: 555−559.

[24] YUAN Ming, ZHENG Zi-qiao. Effects of Zn on the microstructures and mechanical properties of Mg−3Sm−0.5Gd−*x*Zn−0.5Zr (*x*=0, 0.3 and 0.6) alloy [J]. Journal of Alloys and Compounds, 2014, 590: 355−361.

[25] YUAN Ming, ZHENG Zi-qiao. Effects of heat treatment on microstructure and mechanical properties of Mg−2.6Sm−1.3Gd−0.6Zn−0.5Zr alloy [J]. Materials Science and Technology, 2014, 30: 261−267.

[26] LIU Ning-yuan, ZHANG Zhen-yan, PENG Li-ming, DING Wen-jiang. Microstructure evolution and mechanical properties of Mg−Gd−Sm−Zr alloys [J]. Materials Science and Engineering A, 2015, 627: 223−229.

[27] CHE Chao-jie, CHENG Li-ren, TONG Li-bo, CAI Zhong-yi, ZHANG Hong-jie. The effect of Gd and Zn additions on microstructures and mechanical properties of Mg−4Sm−3Nd−Zr alloy [J]. Journal of Alloys and Compounds, 2017, 706: 526−537.

[28] GUAN Kai, EGUSA D, ABE E, ZHANG Jing-huai, QIU Xin, YANG Qiang, MENG Jian. Microstructures and mechanical properties of as-cast Mg−Sm−Zn−Zr alloys with varying Gd contents [J]. Journal of Magnesium and Alloys, 2021, DOI: 10.1016/j.jma.2021.09.013

[29] SAKAMOTO M, AKIYAMA S, OGI K. Suppression of ignition and burning of molten Mg alloys by Ca bearing stable oxide film [J]. Journal of Materials Science Letters, 1997, 16: 1048−1050.

[30] GAO X, ZHU S M, MUDDLE B C, NIE J F. Precipitation-hardened Mg−Ca−Zn alloys with superior creep resistance [J]. Scripta Materialia, 2005, 53: 1321−1326.

[31] XU C, NAKATA T, OH-ISHI K, HOMMA T, OZAKI T, KAMADO S. Improving creep property of Mg−Gd−Zn alloy via trace Ca addition [J]. Scripta Materialia, 2005, 53: 34−38.

[32] CHEN H W, LIU C L, LI Z Q, LI P, ZHANG A P, NIE J F. Effect of Ca addition on microstructures of aged Mg−15Gd−

0.5Zr alloy [J]. Materials Characterization, 2019, 159: 109838.
[33] MO N, MCCARROLL I, TAN Q, CEGUERRA A, LIU Y, CAIRNEY J, DIERINGA H, HUANG Y, JIANG B, PAN F, BERMINGHAM M, ZHANG M X. Understanding solid solution strengthening at elevated temperatures in a creep-resistant Mg−Gd−Ca alloy [J]. Acta Materialia, 2019, 181: 185−199.
[34] ZHAO Hong-liang, HUA Yun-xiao, DONG Xiang-lei, XING Hui, LU Yan-li. Influence of trace Ca addition on texture and stretch formability of AM50 magnesium alloy sheet [J]. Transactions of Nonferrous Metals Society of China, 2020, 30: 647−656.
[35] NAML B, MIRESMAEILI S M, JAMSHIDI F, KHOUBROU I. Effect of Ca addition on microstructure and impression creep behavior of cast AZ61 magnesium alloy [J]. Transactions of Nonferrous Metals Society of China, 2019, 29: 2056−2065.
[36] CHIA T L, EASTON M A, ZHU S M, GIBSON M A, BIRBILIS N, NIE J F. The effect of alloy composition on the microstructure and tensile properties of binary Mg-rare earth alloys [J]. Intermetallics, 2009, 17: 481−490.
[37] LV Shu-hui, MENG Fan-zhi, YANG Qiang, GUAN Kai, MENG Jian. Atomic study on phase transformation of the strengthening phase in a die-casting Mg−Al−La alloy via an intermediate phase [J]. Materials & Design, 2021, 208: 109904.
[38] GREER A L, BUNN A M, TRONCHE A, EVANS P V, BRISTOW D J. Modelling of inoculation of metallic melts: Application to grain refinement of aluminium by Al−Ti−B [J]. Acta Materialia, 2000, 48: 2823−2835.
[39] QIAN M, CAO P, EASTON M A, MCDONALD S D, STJOHN D H. An analytical model for constitutional supercooling-driven grain formation and grain size prediction [J]. Acta Materialia, 2010, 58: 3262−3270.
[40] PALIWAL M, JUNG I H. Microstructural evolution in Mg−Zn alloys during solidification: An experimental and simulation study [J]. Journal of Crystal Growth, 2014, 394: 28−38.
[41] LIANG Yao-Jian, CHENG Xu, WANG Hua-ming. A new microsegregation model for rapid solidification multicomponent alloys and its application to single-crystal nickel-base superalloys of laser rapid directional solidification [J]. Acta Materialia, 2016, 118: 17−27.
[42] MANFRINETTI P, GACHNEIDNER K A. Phase equilibrium in the La−Mg (0−65 at.% Mg) and Gd−Mg systems [J]. Journal of the Less Common Metals, 1986, 123: 267−275.
[43] SACCONE A, DELFINO S, BORZONE G, FERRO R. The samarium−magnesium system: A phase diagram [J]. Journal of the Less Common Metals, 1989, 154: 47−60.
[44] HUTCHINSON C R, NIE J F, GORSSE S. Modelling of the precipitation processes and strengthening mechanisms in Mg−Al(−Zn) automotive alloys [J]. Metallurgical and Materials Transactions A, 2005, 36: 2093−2105.
[45] NIE J F. Effects of precipitate shape and orientation on dispersion strengthening in magnesium alloys [J]. Scripta Materialia, 2003, 48: 1009−1015.

微量 Ca 添加对铸造 Mg−Sm−Gd 基合金显微组织与力学性能的影响

管 凯[1,2]，张景怀[1]，杨 强[2]，李柏顺[3]，巫瑞智[1]，孟 健[2]

1. 哈尔滨工程大学 材料科学与化学工程学院 超轻材料与表面技术教育部重点实验室，哈尔滨 150001；
2. 中国科学院长春应用化学研究所 稀土资源利用国家重点实验室，长春 130022；
3. 长春工程学院 机械与汽车工程学院，长春 130012

摘 要：主要通过透射电子显微镜、高角度环形暗场扫描透射电子显微镜和拉伸测试研究微量 Ca 元素对 Mg−Sm−Gd−Zn−Zr 合金显微组织和力学性能的影响。结果表明，Mg−Sm−Gd−Zn−Zr 合金中主要第二相为 Zn 元素富集的 Mg_3RE 相，Ca 元素添加不仅可以细化晶粒，还可以促进 Mg_5RE 相和溶质原子富集的层错形成。此外，共格界面表明 Mg_3RE 相可以作为 Mg_5RE 相的形核位点，这些均有利于合金力学性能的提高。

关键词：Mg−Sm−Gd 合金；Ca；显微组织表征；力学性能；透射电子显微术

(Edited by Bing YANG)